FIBER ORIENTATION MODELING: A METHOD TO IMPROVE QUANTITATION OF INTRAMYOCELLULAR LIPIDS IN HUMAN SUBJECTS AT 7 TESLA

APPROVED BY SUPERVISORY COMMITTEE

Committee Chairperson's Name _____

Craig R. Malloy, M.D.

Committee Member's Name _____

Manisha Shah, M.D.

Committee Member's Name _____

Sailaja Golla, M.D.

ACKNOWLEDGMENTS

First and foremost, I thank my parents, The Khuu and Nhan Nguyen, for their love and selfless sacrifice. They shaped the person that I am today.

I thank my mentor, Dr. Craig Malloy, for his guidance and tremendous support. His knowledge, passion for research, and enthusiasm for teaching are unparalleled. He is not only an incredible mentor but also a close friend. His achievements set a high standard I aspire to reach.

I thank Dr. Michael McPhaul for his support and for the opportunity to conduct research through the UT Southwestern Medical Student Summer Research Program.

I thank Marilyn English for her wonderful administrative work and my department, Advanced Imaging Research Center, for their continuous support.

I thank Dr. Manisha Shah and Dr. Sailaja Golla for their hard-working, consistent guidance and for serving on my Distinction in Research committee.

I thank Dr. Tejas Shah, Dr. Maria Ramos-Roman, Dr. Malgorzata Marjanska, and Dr. Jimin Ren for their collaborations

Finally, I thank my friends: Rebecca Adelagun, Lily Fathy, and Kimberly Thomas. They made the last few years so memorable.

Support for this study was provided by grant from the National Institute of Diabetes and Digestive and Kidney Diseases T35-DK066141. Support was also provided by the National Institutes of Health (NIH), Grant Number: RR02584 and Department of Defense (DoD), Grant Number: W81XWH-06-2-0046. Special thanks also to the UT Southwestern Medical Student Research Program Fellowship.

FIBER ORIENTATION MODELING: A METHOD TO IMPROVE QUANTITATION OF INTRAMYOCELLULAR LIPIDS IN HUMAN SUBJECTS AT 7 TESLA

by

ANTHONY N. KHUU

DISSERTATION

Presented to the Faculty of the Medical School

The University of Texas Southwestern Medical Center at Dallas

In Partial Fulfillment of the Requirements

For the Degree of

DOCTOR OF MEDICINE WITH DISTINCTION IN RESEARCH

The University of Texas Southwestern Medical Center at Dallas

Dallas, Texas

August, 2009

ABSTRACT

FIBER ORIENTATION MODELING: A METHOD TO IMPROVE QUANTITATION OF INTRAMYOCELLULAR LIPIDS IN HUMAN SUBJECTS AT 7 TESLA

Publication No. 1

ANTHONY N. KHUU

The University of Texas Southwestern Medical Center at Dallas, 2009

Supervising Professor: Craig R. Malloy. M.D.

Background: Increased intramyocellular lipid (IMCL) content in skeletal muscle has been suggested to be a biomarker for insulin resistance. As a noninvasive method of estimating IMCL, ^{1}H MR spectroscopy of muscle fat has been a popular method for measuring the concentration of IMCLs, a goal highly desirable for research in the pathogenesis of type 2 diabetes. Extramyocellular lipids (EMCL) are often considered to be deposited along strands that are parallel to Bo (the applied field) whereas IMCL are assumed to be spherical droplets in the muscle cells' cytoplasm. Resolution between IMCL and EMCL signals mainly results from the angle-dependant bulk susceptibility of the 2 geometric structures. However, IMCL signal is usually contaminated by a broad and asymmetrical EMCL . Conventional fitting methods usually assume that both the IMCL and EMCL signals to be symmetrical, represented by a single Lorentzian, Gaussian or Voigt (hybrid lineshape between Gaussian and Lorentzian) lineshapes.

However, significant asymmetry in the resonance assigned to the methylene protons $(-CH_2-)_n$ in extramyocellular lipids (EMCL) interfered with fitting the spectra. In this work, we explore another approach, named Fiber Orientation Modeling (FOM) by using the bulk susceptibility effect theory to accurately assess the lineshape of EMCL.

Methods: The distribution of EMCL strand orientation at any angle from 0^0 to 90^0 relative to Bo was described by a Gaussian function, centered at a specific angle and a width representing a dispersion of EMCL strands. The chemical shift ω from each strand was translated by the well-known orientation dependence interaction $\omega = 3\cos^2\theta-1$, where θ is the angle between EMCL and the applied field. As the result, the location and amplitude of individual curves representing each strand could be derived. Depend on the aforementioned Gaussian distribution, the combination of these individual curves generated a unique EMCL shape. In this work, spectral simulations were generated using muscle fiber orientation reported previously. The phantom experiment with a fat cylinder (representing EMCL) submerged in Intralipid^{TM} solution (representing IMCL) was also performed to determine the maximal shift at 0^0 and 90^0. Under IRB approval, single voxel and chemical shift images were acquired from soleus and gastrocnemius muscle of healthy human subjects at 7T (Phillips Medical system, Cleveland, Ohio). All the spectra were fitted with the hybrid Voigt lineshape and the experimental lineshape.

Results: In simulated spectra with dominant angle of 0^0 to the applied field and little dispersion, fitting with the Voigt lineshape accurately determined IMCL/EMCL ratio over a range of different linewidths. Increasing dispersion and central angle caused overestimation of

IMCL/EMCL ratios, up to three-fold when fitted with the Voigt lineshape. The error was substantially reduced using our method. The improvement is also observed in phantom spectra and human spectra. Estimates of [IMCL]/[EMCL] were significantly improved by including variations in fiber orientation in the lineshape analysis (fiber orientation modeling, FOM). Calculated soleus [IMCL] using FOM, 4.43 ± 2.32 mmol/kg wet weight, was lower compared to most previous reports in soleus. The average orientation of EMCL was calculated to be 35^0 relative to Bo with a dispersion width of 24^0

Conclusion: Since prominent asymmetrical EMCL signal tends to contaminate into IMCL region, this interaction results in the amplitude-dependence of IMCL signal on the average orientation and dispersion of EMCL. As the result, the use of symmetrical lineshape tends to overestimate the IMCL signal if all strands of EMCL are not parallel to Bo and one another. By accounting for the angular dispersion& orientation, the fit would improve both the residual and the IMCL estimate.

.

TABLE OF CONTENTS

PRIOR PUBLICATIONS & PRESENTATIONS

Anthony Khuu, Jimin Ren , Ivan Dimitrov, Donald Woessner, James Murdoch, A. Dean Sherry, Craig R. Malloy (2008). Orientation of lipid strands in the extracellular compartment of muscle: Effect on quantitation of intramyocellular lipids. *Magnetic Resonance in Medicine* 61(1):16-21.

Anthony Khuu, Jimin Ren, James Murdoch, Ivan Dimitrov, Donald Woessner, A. Dean Sherry, Craig Malloy (2008). Angular Dispersion and Average Orientation of Bulk Triglycerides: Influence on the Proton Lineshape from Extramyocellular Fat. *Proceedings of the International Society for Magnetic Resonance in Medicine 2008.*

Anthony Khuu, Craig R. Malloy (2008). Modeling ^{1}H MRS Signal lineshape from Extramyocellular Lipids (EMCL): Influence of EMCL signal on the Estimate of Intramyocellular Lipids (IMCL) at 7T. 46th Medical Student Research Forum, UT Southwestern Medical Center, Dallas, Texas.

Submitted Manucripts/Abstracts/Presentations:

Manisha Shah, Anthony Khuu, Shalini Reddy, Craig Malloy (2009). Skeletal Muscle Metabolism in Congestive Heart Failure. American Heart Association. Manuscript submitted for publication

Jimin Ren, Anthony Khuu, Craig Malloy (2008). ^{1}H NMR Spectroscopy in Skeletal Muscle. Program 4th Phillips 7T User Meeting. Eidgenössische Technische Hochschule (Swiss Federal Institute of Technology) Zurich, Switzerland.

Anthony Khuu, Jimin Ren, Pi-Yu Zhao, James Murdoch, Ivan Dimitrov, Don Woessner, A. Dean Sherry, and Craig Malloy (2008). Angular Dispersion of Lipids in the Extracellular Compartment of Muscle: Effect on Quantitation of intramyocellular Lipids. Poster Session at the 46th Medical Student Research Forum, UT Southwestern Medical Center, Dallas, Texas

.

LIST OF FIGURES

LIST OF TABLES

LIST OF DEFINITIONS

FATTY ACID –a carboxylic acid often with a long unbranched aliphatic tail (chain), which is either saturated or unsaturated.

MRI–noninvasive diagnostic technique that uses nuclear magnetic resonance magnetic resonance to produce cross-sectional images of organs and other internal body structures

MRS – The MR signal produces a spectrum of resonances to measure the levels of different metabolites in body tissues.

TESLA (unit) – the SI derived unit of magnetic field.

T1–known as Spin-lattice relaxation time is a time constant in Nuclear Magnetic Resonance and Magnetic Resonance Imaging

T2– known as Spin-spin relaxation time is a time constant in Nuclear Magnetic Resonance and Magnetic Resonance Imaging

IMCL – Intramyocellular lipid

EMCL – extramyocellular lipids

SOLEUS – powerful muscle in the back part of the lower leg (the calf), running from just below the knee to the heel, and is involved in standing and walking

GASTROCNEMIUS– a powerful superficial muscle that is in the back part of the lower leg (the calf). It runs from its 2 heads just above the knee to the heel, and is involved in standing and walking.

CHAPTER ONE
Introduction

Although found primarily in adipose tissue, lipids are also present in other tissues such as liver and muscle. In skeletal muscle, one form of triglycerides, intramyocellular lipid (IMCL), exists as fat droplets in the muscle cell's cytoplasm and is utilized as energy source during high demand. Being considered a risk factor of insulin resistant, a reliable method of IMCL analysis is highly desirable for research in lipid metabolism and diabetes pathogenesis. Recently, the use of volume localized ^{1}H magnetic resonance spectroscopy (MRS) as a non-invasive method to study skeleton muscle *in vivo* has provided a fast and highly sensitive method for IMCL analysis [1-5]. In these spectra, chemical shift resolution of the ^{1}H signal from intra- vs. extracellular fat occurs because the magnetic field inside a diamagnetic structure depends on its shape, orientation, and magnetic susceptibility [6 – 9]. The use of ^{1}H MRS is often assumed that intramyocellular lipids (IMCL) are approximately spherical droplets and that extramyocellular lipids (EMCL) may be modeled as strands of fat [3,10]. This model have has been confirmed in phantoms [11], animals [12] and human subjects [3, 13].

The dominant methylene proton signal from (-CH2-)n is usually used to assess the IMCL content. However, both the IMCL and EMCL signals must be fit because a strong signal from interstitial fat between muscle fibers (extramyocellular lipid - EMCL), especially in obese patients, usually contaminates the spectral region of interest, reducing the accuracy of IMCL assessment [1-2, 5, 15-23]. To get a reliable result, conventional fitting methods usually require an optimal separation of the IMCL and EMCL as well as employing the assumption that both IMCL and EMCL peaks are symmetrical. Since EMCL exists as fat septa along muscle fibers,

the EMCL spectra is highly variable in shapes, depends strongly on the angle between fat septa and the magnetic field Bo. If fitting a markedly asymmetrical EMCL spectra by a single, symmetrical lineshape (conventionally Lorentzian, Gaussian or Voigt lineshapes are used), the IMCL line may be systematically over-or underestimated [2]. In reality, optimal chemical shift resolution is only observed in the anterior tibialis muscle where EMCL strands are thought to be parallel to one another and to Bo [3, 5, 13 – 15]. Asymmetry of the signal from EMCL has usually been observed in other types of muscle [3] and an asymmetrical EMCL with a large upfield component seems to be the prevalence form rather than the exception [3, 5, 24]. Several investigators have also remarked on the difficulty and inaccuracy of fitting spectra from muscles other than the anterior tibialis [3, 24].

Higher magnetic fields promise improved chemical shift dispersion and sensitivity, but in principle line-broadening due to susceptibility-induced static field inhomogeneities may offset these benefits [3]. Consistent with this prediction, in our initial studies of skeletal muscle at 7T, conventional line fitting was unsatisfactory because of marked asymmetry in the methylene resonance from EMCL. We have explored several methods documented in the literature to resolve this problem. A method of separation IMCL from EMCL by obtaining magnetic field distribution (MFD) with a reference lipid spectrum obtained from bone marrow was suggested by Steidle and Machann [24]. In this approach the IMCL part of the MFD was fixed with a Gaussian line, using the same linewidth as of creatine. Then the amplitude of IMCL was varied to obtained a smooth but not necessarily symmetrical EMCL. The disadvantage of this method was the time-consuming requirement of visual observation and input by operator. Another approach by Weis and Courivaud was to obtain a reference EMCL spectrum by fitting a series of pure EMCL spectra [1]. This approach, however, still utilized symmetrical fitting lineshapes and

based on the assumption that fiber orientation presented in the reference spectrum is similar to that from the spectra of interest.

In this work, we explore another approach in separation EMCL and IMCL effectively termed fiber orientation modeling (FOM). Our method employs the well-known dipolar interaction $3\cos^2\theta-1$, where θ is the angle between the structures and the magnetic field Bo, with multiple symmetrical Lorentzian curves to generate the shape of EMCL. We utilize a least-squared fitting algorithm, incorporating prior knowledge, to fit simultaneously six overlapping components of the region of interest: EMCL and IMCL peaks from methyl groups, EMCL and IMCL peaks from methylene groups, and EMCL and IMCL peaks from beta carbons adjacent to the carboxyl groups. This technique is especially applicable in severely distorted EMCL peaks with large overlapping region with IMCL signals. Simulated spectra and data from human subjects at 7T were analyzed. Based on reported fiber angles [25], the predicted ^{1}H spectrum from extracellular fat was a complex lineshape that is underspecified by symmetric functions. The IMCL signal was overestimated using symmetric lineshapes for fitting when the EMCL strands were not parallel to one another. FOM was used to resolve IMCL from EMCL signals, to estimate the average orientation of lipids in the extracellular compartment, and to determine [IMCL].

CHAPTER TWO
Theory and Formulation

THEORY

In muscle tissue, lipid is stored as extramyocellular lipid (EMCL) and intramyocellular lipid (IMCL). IMCL is accumulated inside skeletal muscle cells as small (0.5 μm in diameter) homogenous fat droplets [5]. As a result of the geometric symmetry of the fat droplets, the signals from IMCL are symmetric and independent orientation in the magnetic field. IMCL droplets are thought to be metabolically active and to have a fast turn-over rate, being used usually within several hours [22]. EMCL, on the other hand, is less metabolically active interstitial adipocytes nested in septa between muscle fibers. Due to this geometrical arrangement of EMCL layers or strands along muscle fibers, EMCL signals are affected by the orientation-dependent magnetic susceptibility effect due to inhomogenous field [11]. Depending on the fiber architecture of a muscle, EMCL signals can be very broad and markedly asymmetrical [10].

The influence of orientation, the angle q relative to Bo, on the field inside a cylindrical biological object is typically modeled as 3cos2 q - 1 [26], an approximation that has been confirmed experimentally [8, 11]. Based on the works by Szczepaniak et al. [12] with formalism derived by Chu et al. [8] that demonstrated how bulk magnetic susceptibility effects influence location, shape and size of EMCL, the bulk susceptibility can be calculated as details below.

Within the highly symmetrical compartment (sphere, or cylinder), the field Bi can be express as (i represent the compartment):

$$B_i = (1+D)\, Bo \qquad (1)$$

With D is a function of magnetic susceptibility of substances (w for water and f for fat) in different compartments and orientation o f those compartments:

For a spherical compartment:

$$D_{internal} = \chi w /3 \qquad (2)$$

$$D_{external} = \chi w /3 \qquad (3)$$

For a parallel cylinder:

$$D_{internal} = \chi f /3 \qquad (4)$$

$$D_{external} = \chi w /3 \qquad (5)$$

For a perpendicular cylinder:

$$D_{internal} = (\chi w/2 - \chi f/6) \qquad (6)$$

$$D_{external} = \chi w/3 \qquad (7)$$

The relative difference in local magnetic field can be calculated as

For a spherical compartment, from (1) & (2, 3):

$$\Delta B_{IMCL} = 0$$

For a parallel cylinder, from (1) & (4, 5):

$$\Delta B_{EMCL//} = \frac{B_o * (X_f - X_w)}{3}$$

For a perpendicular cylinder, from (1) & (6, 7):

$$\Delta B_{EMCL\perp} = \frac{-B_o * (X_f - X_w)}{6}$$

Using diamagnetic susceptibility values of water χw=-9.05 and compound fat χf≈-8.44 [8], the values can be calculated $\Delta BEMCL_{II}$≈0.26 and $\Delta BEMCL_{\perp}$≈-0.13
Based on this model, confirmed by the phantom experiment by [11], IMCL always had the same resonance, whereas EMCL resonance shifted with range from +0.20 to +0.26 ppm upfield to -0.1 ppm to -0.13 ppm downfield with respect to IMCL. The maximum shift +0.26 ppm resulted from parallel orientation while the minimum shift -0.13 ppm resulted from a perpendicular orientation. EMCL resonance crossed over IMCL resonance at magic angle of 55^{o} (Figure 1).

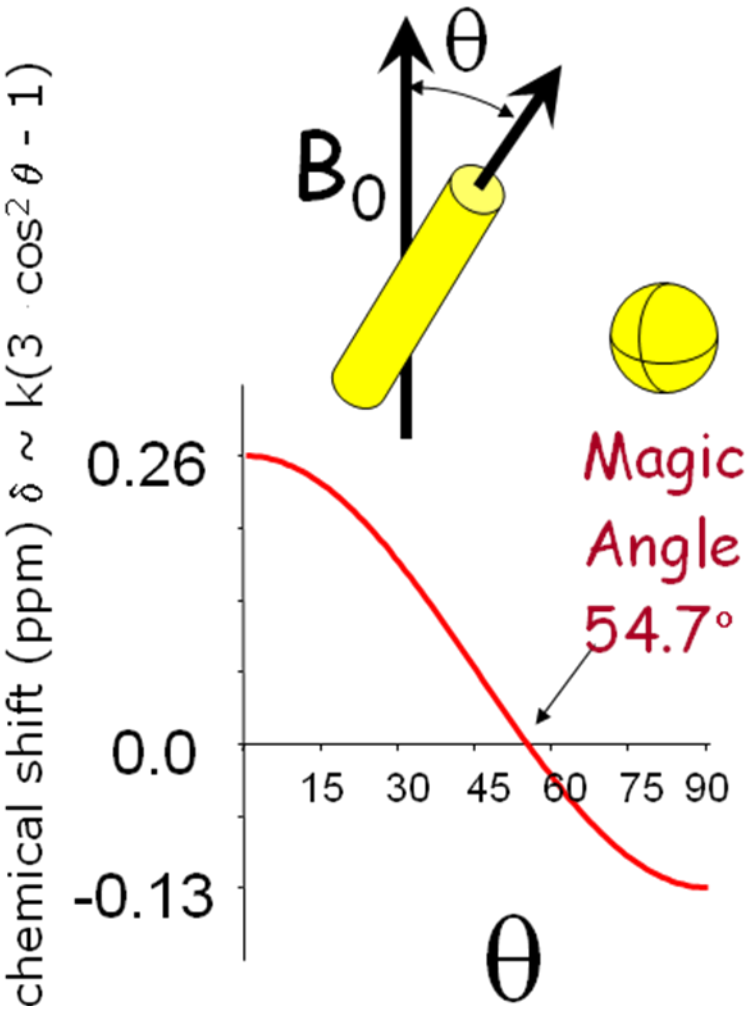

Figure 1: Relationship between chemical shift and orientations

Since EMCL strands may not be parallel to Bo, the **^{1}H** signal may be asymmetric

and will overlap with IMCL, depending on orientation.

FORMULATION

Each muscle type has a unique and highly organized fiber structure. The muscle "pennation angle" between muscle/fat fibers and the main axis of the muscle has been shown to be uniform between subjects for the same muscle group [25]. Since EMCL deposits along muscle fibers, each resonance from EMCL is influenced by this unique angle. Because the "pennation angle" is fairly uniform, we hypothesize that EMCL signals follows a bell-shaped normal distribution around the "pennation angle". Hence a Gaussian lineshape is an appropriate model for the distribution (P):

$$P = A * e^{-\frac{(x-B)^2}{C^2}}$$

With A is the height, B is the position and C is the width

Ten Lorentzian curves with equal width are created to span the entire EMCL range. Each curve represents a ten degree of angle shift (0^0, 10^0, 20^0,…, 90^0). The location L of each curve along the ppm scale is determined by the equation 3cos2 q – 1 as follow:

E is the location EMCL methylene peak, I is the location IMCL methylene peak:

$$3T * \cos^2(90^o) - O = I - \frac{(E - I)}{2}$$

$$3T * \cos^2(0^o) - O = E$$

As the result, the location L of each curve along the ppm scale is determined as:

$$\boldsymbol{L = 3T * \cos^2(angle) - O}$$

$$\boldsymbol{T} = \frac{(E + O)}{3}$$

$$\boldsymbol{O} = -I + \frac{(E - I)}{2}$$

From there, the pre set locations of 10 curves can be determined. For each curve that represents a group of EMCL strands, the amplitude of the curve is being determined based on the distribution P. The curve is represented by a Lorentzian equation:

$$F = \frac{P * W^2}{W^2 + (x - L)^2}$$

With P is the amplitude, L is the location and W is the width

So for example, curve #1 (f1) with location L1 (ppm), linewidth W1 along angle distribution P is:

$$f1(x) = \frac{A * e^{-\frac{(x-L1)^2}{C^2}} * W1^2}{W1^2 + (x - L1)^2}$$

By simulating fitting these ten curves together, the summation of these curves will yield a characteristic curve that approximates the EMCL reliably with minimal residues.

The model, illustrates schematically in Figure 2 and 3, is termed fiber orientation modeling (FOM).

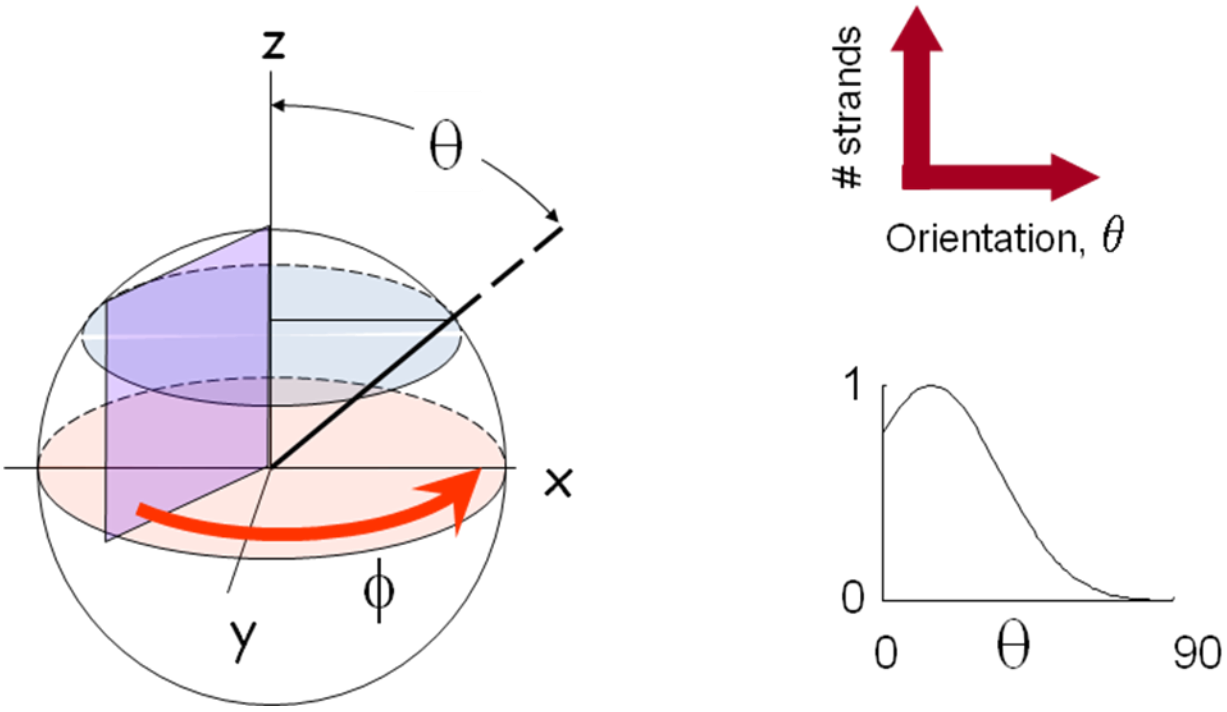

Figure 2: Assumptions of the model:

1) Orientation of an EMCL Fiber is described by θ (relative to Bo) and ϕ (around Bo
2) Distribution of orientations can be described by a Gaussian function.

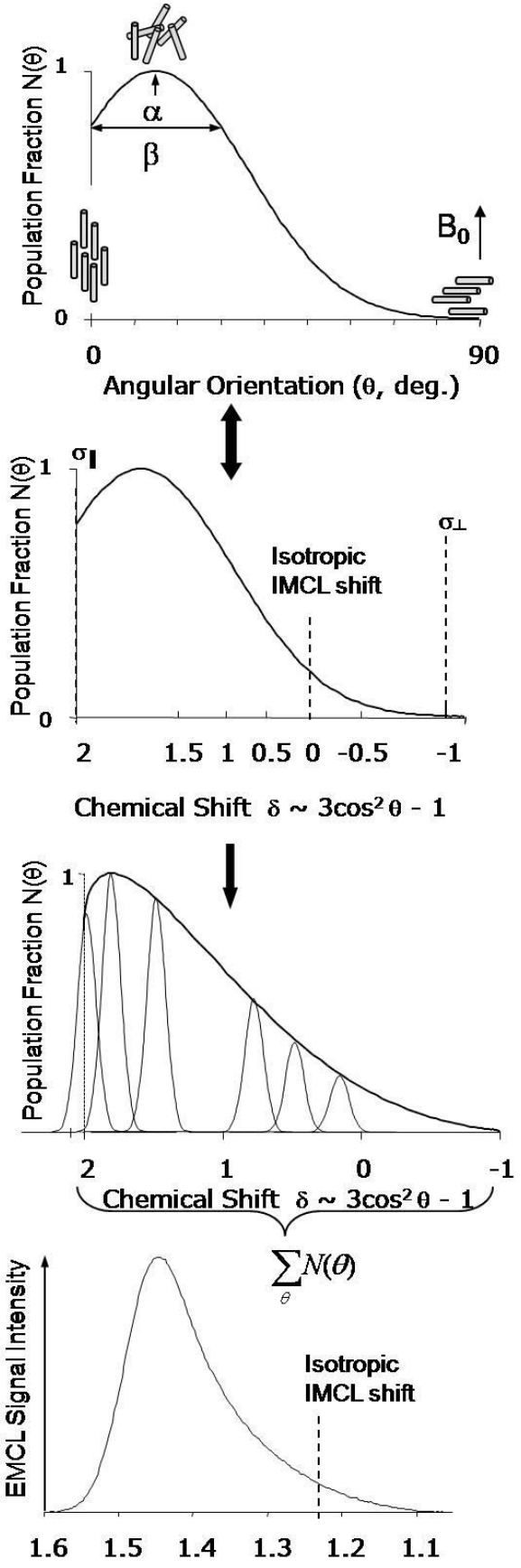

Figure 3: Schematic Description of Fiber Orientation Modeling.
In this example, the Gaussian distribution of extracellular fat (panel A) was $\alpha = 15°$ and $\beta = 30°$. The chemical shift for each angle was calculated and represented as a Gaussian line with the appropriate amplitude. Panel A also shows a schematic of fiber orientation. Panel B illustrates conversion of orientation, θ, to ppm. Panel C shows a linear axis in ppm plus amplitude-scaled individual signals of equal linewidth. The final simulated spectrum, D, is the sum of 91 such resonances.

CHAPTER THREE
Study Design

SIMULATION OF LIPID STRAND ANGLES AND COMPUTER-GENERATED SPECTRA

Based on the aforementioned formulation, computer-simulated spectra can be created. In the current model, the number of protons (N) in a lipid strand at an angle (θ) relative to Bo represents the sum of all strands for that value of θ and every value of ϕ, with an angle θ which varies from 0° to 90° and describes the orientation relative to Bo, and an angle ϕ which varies from 0° to 360° and describes the orientation around the axis of Bo. $N(\theta)$ is described as a Gaussian distribution with a dominant angle (α) and a width of the distribution (β) with a range from 0 to 90°, as $N(\theta) = \exp(-((\theta - \alpha)/\beta)^2)$. The width of the distribution characterizes the dispersion in orientations of fatty strands within the voxel relative to Bo. Each source is assumed to produce a single resonance with a Gaussian lineshape and chemical shift, $3\cos^2\theta - 1$. The amplitude of each resonance was determined by the relative amount of lipid at that angle θ.

By incrementing θ and summing the results, a spectrum can be generated to simulate ^1H NMR spectra. To explore the effect of orientation and dispersion on the observed spectrum, simulations were performed assuming [IMCL] / [EMCL] = 0.5. The chemical shift was scaled so the maximum range of chemical shift was 0.36 ppm corresponding to a change in orientation, θ, from 0° to 90°. The concentration of the seven predominant fatty acids [29] was used to calculate the relative area of the methyl resonance, the $(-CH_2-)_n$ resonance, and the resonance from the protons β to the carbonyl, 1.0 : 6.6 : 0.67. The EMCL signal was generated as the sum of signals of equal linewidth from 91 sources with equal increments in θ from 0° to 90°. Different combinations of central angles (α) and dispersions (β) were generated using orientations

ranging from 0°, approximately representative of anterior tibialis, to 45° approximately representative of the gastrocnemius [25].

HUMAN MR SPECTROSCOPY AND IMAGING

The protocol was approved by the Institutional Review Board of UT Southwestern Medical Center. Healthy sedentary adults (2 females and 7 males) age 21 – 68 years (average 44 years, without known vascular disease or diabetes) were studied supine in a 7T system (Achieva, Philips Medical Systems, Cleveland, OH). Spectra and images were acquired with a partial-volume quadrature transmit / receive coil. Axial, coronal and sagittal T2-weighted turbo spin echo images were acquired from the left calf muscle with field-of-view FOV 180 x 180mm, TR 1500 ms, TE 75 ms, turbo factor 16, and number of acquisitions 1. The T2 weighted planar image data were used to reconstruct 3D images using maximum intensity projection (MIP). Parameters for the single-voxel STEAM spectra were: voxel size 1.0 mL, TR 2000 ms, TE 20 ms, spectral bandwidth 4000 Hz, number of points 4096, number of acquisitions 192, with water suppression). The volume of interest was chosen to minimize obvious extramyocellular fat signal [3, 4].

Subjects were instructed to move slowly to avoid any physiological effects associated with rapid changes in the static magnetic field. The entire scanning session was 60 min or less and it was well-tolerated by all subjects. All subjects were interviewed after the exam and again at 24 hours after the exam. All subjects specifically denied dizziness, nausea, vertigo, headaches or visual changes.

A total of 18 spectra (2 spectra each from 9 subjects) were acquired. Spectra acquired generally had good signal to noise rations. Poor quality spectra with excessive signal-to-noise

ratios, extreme peak overlapped or rugged irregular peaks were discarded. One spectrum from soleus was discarded based on these criteria. 17 spectra from 9 patients were fitted and data were gathered for analysis.

FITTING PROCEDURE FOR ^{1}H NMR SPECTRA

Spectra from all two experiments were fitted using a nonlinear least squares algorithm (lsqcurvefit) written in MATLAB (The MathWorks, Natick, MA). The graphic-user fitting interface (Figure 4) was written to simultaneously fit six overlapping components of the region of interest from 0.5 to 1.9 ppm. In order to compare the accuracy of our newly derived lineshape FOM, the line was compared against Voigt lineshape. Since all three lines, Gaussian, Lorentzian and Voigt was popular among NMR community as a tool for fitting spectrum, fitting results from Voigt (hybrid line between Gaussian and Lorentzian) were considered to be control groups. In the control group, spectra were fit using a Voigt lineshape (ACD/Specmanager, Advanced Chemistry Development, Inc.) to estimate the resonances between 0.5 - 1.9 ppm: the IMCL and EMCL signals from protons in the $-CH_3$ groups, $(-CH_2-)_n$ groups, and the $-CH_2-$ group β to the carbonyl ($-CH_2-CH_2-COO-$).

In the experimental group with the same set of spectra, three resonances from IMCL were fit as Voigt lineshapes and assigned to the protons β to the COO, protons in the bulk methylene resonance, $(-CH_2-)_n$, and protons in the CH_3. Three other resonances from EMCL were shifted downfield by approximately 0.2 ppm. These resonances were fit simultaneously using FOM. The signal from the protons β to COO in IMCL ("buried β") overlaps with the $(-CH_2-)_n$ methylene signal from EMCL. Because the β group ($-CH_2-CH_2-COO-$) has two contributing proton compare to methyl group with three protons, a 2/3 scaling factor was used. The two

EMCL methylene resonance and the methyl resonances were each represented as the sum of 11 resonances of equal linewidth originating from lipid strands oriented at equal increments from 0 to 90° since additional resonances did not improve the fitting significantly and increased computation time. The chemical shift of the IMCL resonance was assumed to be located at same chemical shift as an EMCL oriented at 54.7°.

Three sets of simulated spectra for each combination of α (central angles) and β (dispersions) were fit using a Voigt lineshape. The same dataset was fit using the FOM least-squares algorithm.

Spectra from the gastrocnemius and soleus from healthy subjects were also analyzed by FOM and Voigt fitting in the region 0.5 to 1.9 ppm and also in the region around the CH_2 resonance of creatine [3]. The concentration of IMCL triglycerides was calculated as recommended in [3]. Resonance areas were corrected for differential relaxation losses as described [27] assuming a T1 and T2 for creatinine of 1050 and 74 msec, respectively, and measured T1 and T2 at 7T in human marrow or subcutaneous fat, 540 and 65 msec (unpublished observations).

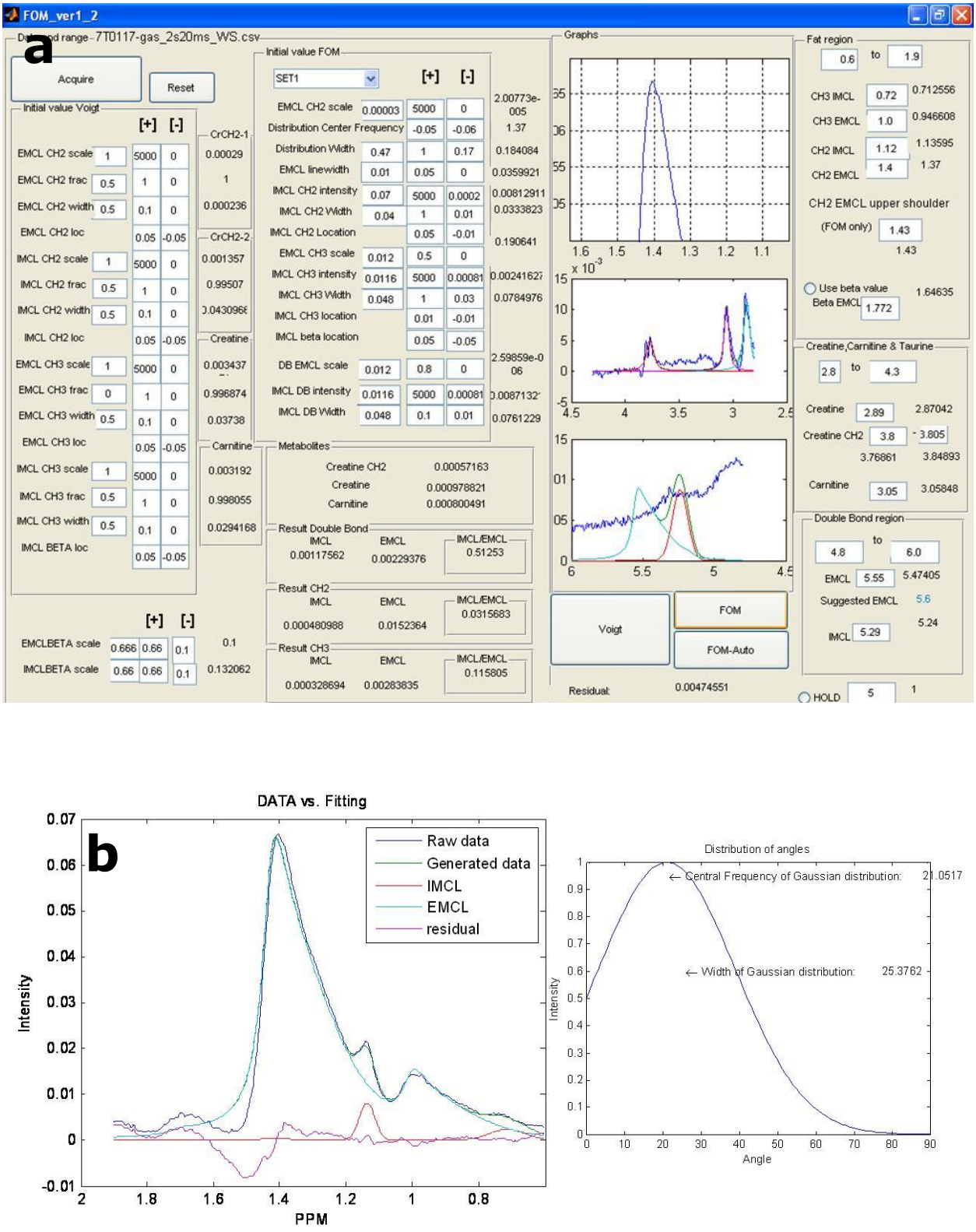

Figure 4: Fiber orientation Modeling (FOM) fitting interface

CHAPTER FOUR
Result

FITTING OF SIMULATED SPECTRA

The effect of variable orientation on the simulated ^{1}H NMR spectrum of muscle is illustrated in Figure 5 for [IMCL] / [EMCL] = 0.5. The spectrum in the upper left panel demonstrates optimal resolution because the dominant angle of extracellular fibers, α, is 0° relative to Bo and the dispersion in orientation, β, is minimal. Consequently the [IMCL] / [EMCL] by inspection is approximately 0.5. With increasing dispersion (β), moving down the column, the extracellular signal becomes asymmetric and the apparent amplitude of the IMCL increases. Since the asymmetry caused by variable orientation occurs upfield to the EMCL signal and is superimposed on the IMCL signal, it may not be obvious that the spectrum in the lower left panel was also generated with [IMCL] / [EMCL] = 0.5. The effects of changing the dominant angle, α, from 0° to 15° to 30° relative to Bo is illustrated by moving horizontally across Figure 5. Increasing the dominant angle relative to Bo is equivalent to reducing resolution and as a result the spectrum in the upper right shows poorer resolution but the apparent [IMCL] / [EMCL] remains about 0.5. Because of the combined effects of reduced chemical shift resolution and variable orientation, [IMCL] / [EMCL]s appear much greater than 0.5 in the lower right panel.

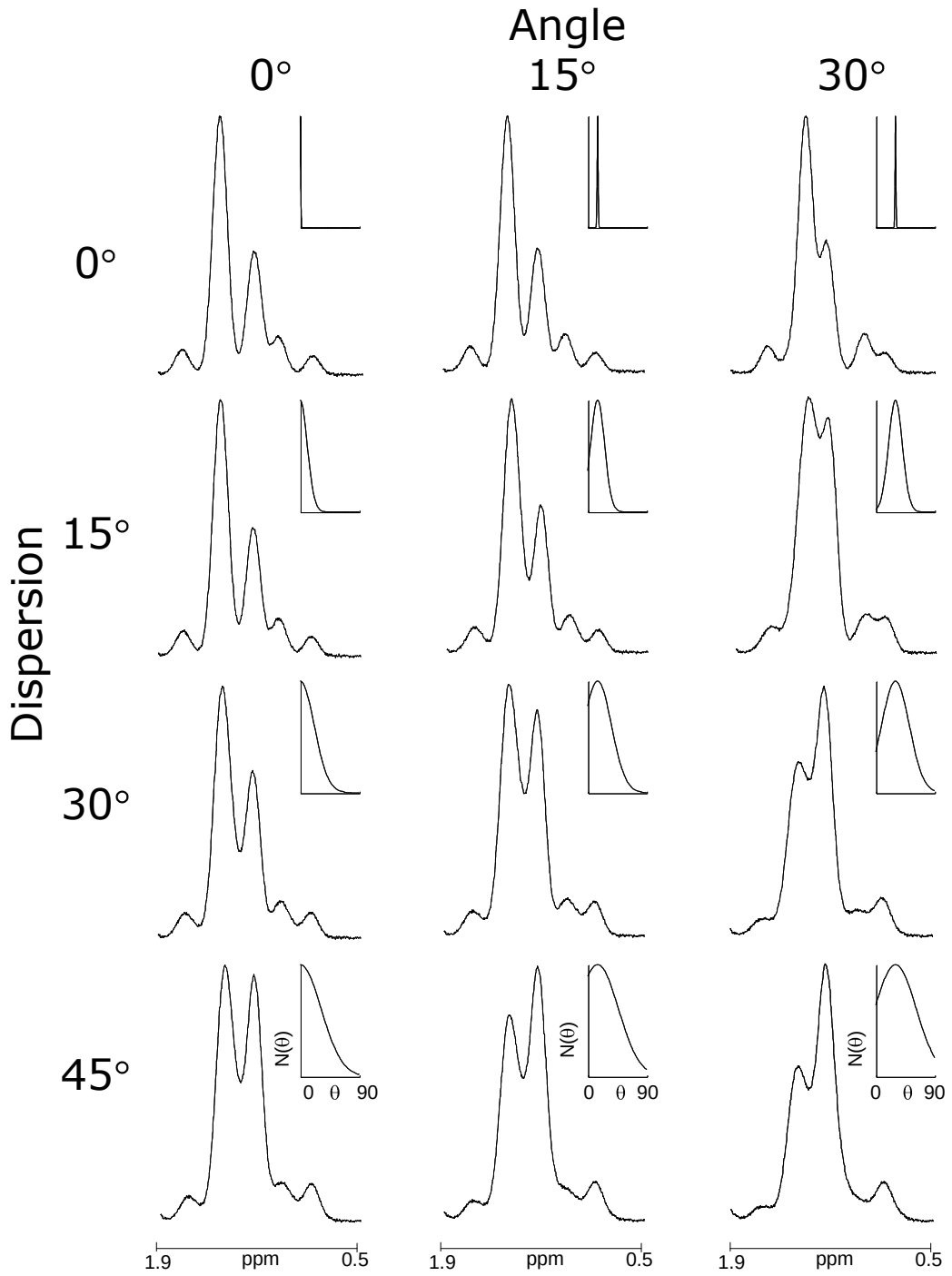

Figure 5: Computer-Generated Spectra: Influence of Orientation on ^{1}H NMR Spectra for Constant [IMCL] / [EMCL]. The ratio of IMCL/EMCL was fixed at 0.5. As the dominant angle α relative to Bo changes from 0° - 30°, the chemical shift resolution is reduced. With increasing dispersion β, the EMCL signal broadens asymmetrically.

Simulated spectra were analyzed assuming that each resonance could be represented as the sum of a Lorentzian and Gaussian line (Voigt lineshape). The effects of variable orientation on estimated [IMCL] / [EMCL] are shown in the upper panel of Figure 4. If dispersion is minimal, less than ~ 15°, curve fitting with the Voigt lineshape returned [IMCL] / [EMCL] accurately. However, [IMCL] / [EMCL] was significantly overestimated at higher dispersion if using Voigt fitting.

The same data set was analyzed by FOM and the results are shown in the lower panel of Figure 6. Unlike fitting with the Voigt lineshape, there was little effect of variation in the central angle on the estimated [IMCL]/[EMCL]. Therefore, all results for each orientation angle were aggregated (lower panel, Figure 4). More importantly, there was no effect of dispersion on the estimated [IMCL] / [EMCL]. FOM underestimated [IMCL] / [EMCL] by 10 –20%

.

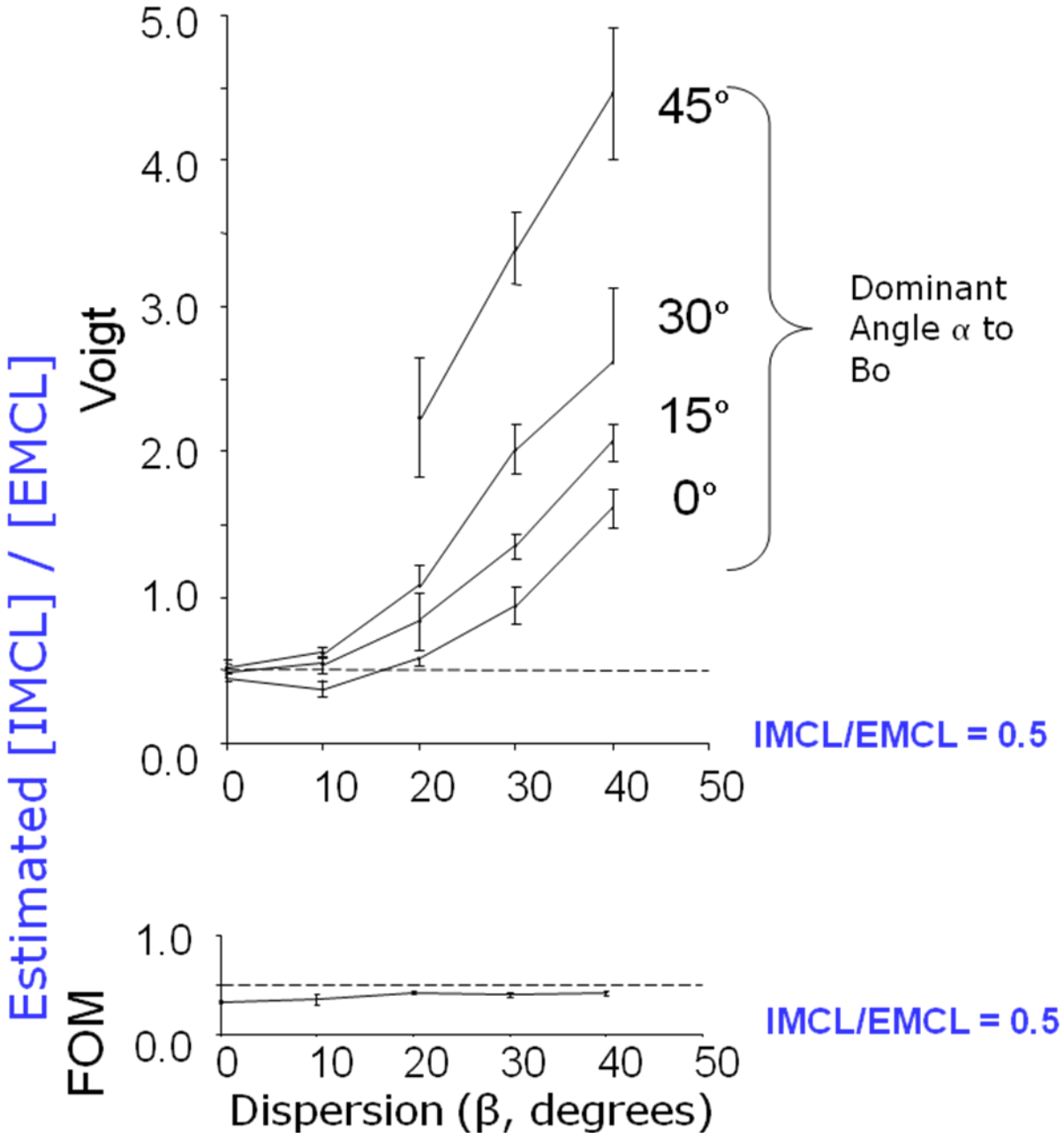

Figure 6: Comparison of Voigt Fit and Fiber Orientation Modeling.
Simulated spectra with [IMCL] / [EMCL] = 0.5 were generated using different central angles and dispersions. Typical spectra are shown in Figure 4. When the spectra were analyzed using Voigt lineshape, [IMCL] / [EMCL] was overestimated except when angular dispersion was small (upper panel). The Dominant Angle and Dispersion Strongly Interacted with the Estimated [IMCL]/[EMCL] when Fit with a Voigt Function. There was no effect of dispersion on the accuracy of estimated [IMCL] / [EMCL] using the FOM algorithm (lower panel).

HUMAN CALF MUSCLE SPECTRA

The three-dimensional structure of extracellular fat in skeletal muscle is complex. In Figure 7, a conventional cross sectional image (A) and two MIP images for fat volumetric distribution (B and C) are shown. The bright regions in the MIP images, reconstructed from T2-weighted images, represent subcutaneous fat (the large curved plate in B), bone marrow of the fibula (the thickest cylinder in C) or strands of extracellular fat between muscle fibers (the finer strips in C). If the lower leg is positioned with the tibia or fibula approximately parallel to Bo, most strands of extracellular fat are not parallel to Bo and are not parallel to one another.

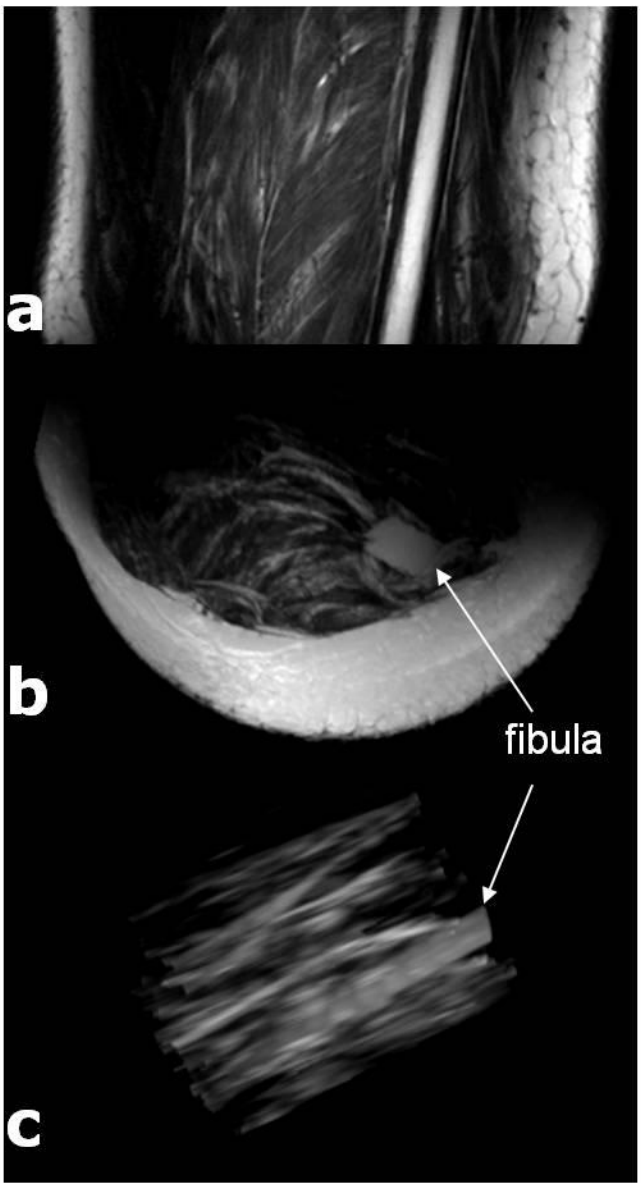

Figure 7: Coronal, Axial and Maximal Intensity Projection Images of the Calf.

Panel A shows a typical longitudinal image with substantial subcutaneous fat, fat strands throughout, and marrow fat in the fibula. The axial image is Panel B. After removal of subcutaneous fat, C, the variability in orientation of the extracellular fat relative to fibula marrow is evident.

The difference in curve fitting by FOM compared to Voigt fit is illustrated in Figure 8, a spectrum from the soleus of a healthy volunteer. The observed spectrum from 0.5 - 1.9 ppm is shown in the upper panel. The estimated EMCL and IMCL signals from methyl, bulk methylene $(-CH_2-)_n$ and CH_2 β to COO, as well as the residual, are shown assuming Voigt lineshape. There were two effects of FOM. The residual was reduced, but more significantly the estimated [IMCL] / [EMCL] was reduced from 0.91 to 0.25, a rather dramatic difference. In this example the dominant orientation (α) of extracellular triglycerides was 23° relative to Bo with a dispersion width (β) of 38°.

[IMCL] / [EMCL] was measured by Voigt fitting and by FOM in all subjects in both the gastrocnemius and the soleus (Figure 9). The average [IMCL] / [EMCL] was 0.41 ± 0.31 (mean ± s.d.) in the gastrocnemius and 0.67 ± 0.26 in the soleus when spectra were analyzed by Voigt fitting. However, the average value for [IMCL] / [EMCL] was significantly lower in both the gastrocnemius (0.18 ± 0.11) and in the soleus (0.29 ± 0.06) when fit with FOM. In both muscle groups, FOM returned a value for [IMCL]/[EMCL] that was about 44% of the results from conventional fitting and the variance was smaller. Presumably the amount of extracellular fat in each voxel was very roughly similar since we followed the standard practice of selecting "lean" voxels for data acquisition. The fact that [IMCL] / [EMCL] was significantly lower when estimated by FOM compared to a symmetric function suggests that the overestimation of [IMCL] when fit with a symmetric function was due to selection of regions with variable fiber orientations.

The ratio [IMCL]/[EMCL] was determined because signal from lipids in both compartments generally overlap and must be fitted. However, the most interesting biological information is probably not this ratio but rather the concentration of intracellular lipids. Using

the creatine signal as an internal concentration standard and assuming [creatine] is 30 mmol/kg wet weight in healthy subjects [3], the [IMCL] can be determine:

$$[IMCL] = 30 * \frac{3}{59.7} * \frac{Area\ under\ the\ curve\ of\ methylene\ CH_2}{Area\ under\ the\ curve\ of\ creatine\ CH_3}$$

From analysis with the Voigt lineshape, the concentration of IMCL was 8.31 ± 7.84 mmol/kg wet weight in the gastrocnemius and 10.65 ± 3.43 mmol/kg wet weight in the soleus. Using FOM, the concentration of IMCL was significantly lower in both muscle groups, 3.73 ± 2.19 mmol/kg wet weight in the gastrocnemius and 4.43 ± 2.32 mmol/kg wet weight in the soleus (see Table 1).

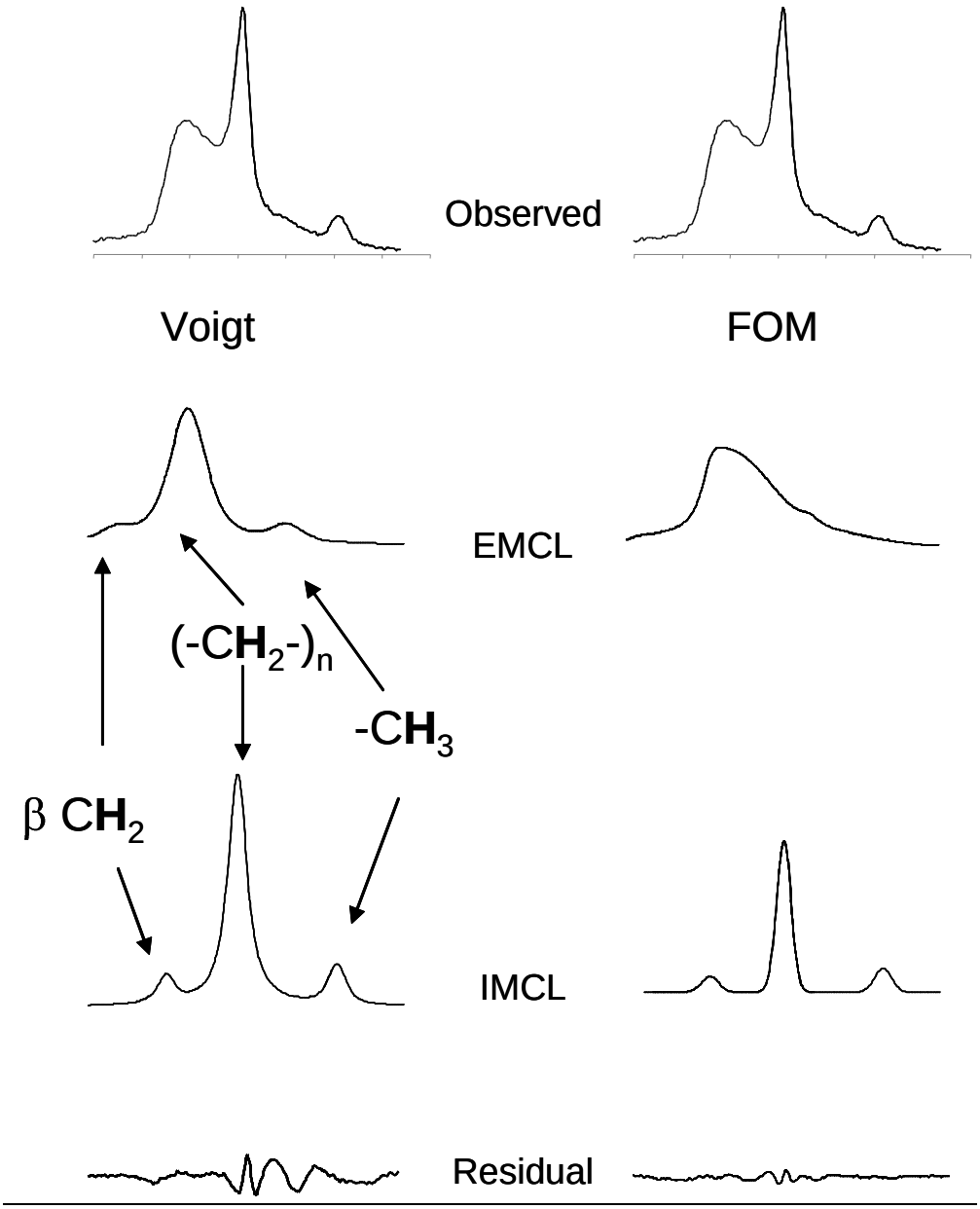

Figure 8: Analysis of a ^{1}H NMR Spectrum Using a Voigt Function vs. Fiber Orientation Modeling.

The ^{1}H NMR spectrum between 0.6 and 1.9 ppm from the gastroc-nemius was fit using a Voigt function (left panel) and FOM (right panel). FOM Yielded a Smaller Residual and Lower [IMCL]/[EMCL]

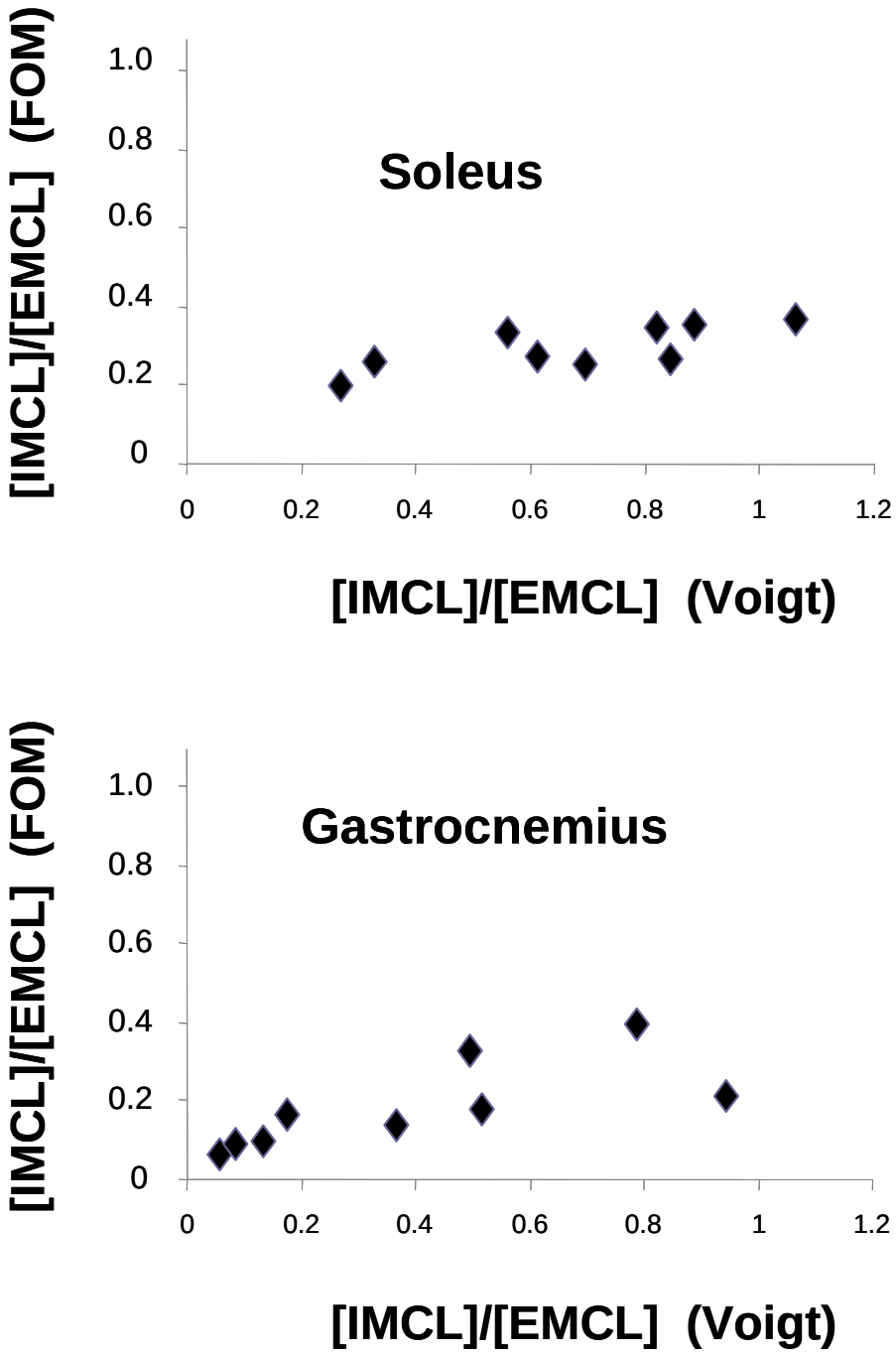

Figure 9: Comparison of Fitting with a Voigt Lineshape Compared to Fiber Orientation Modeling.

The ratio of IMCL to EMCL was calculated for the soleus (upper panel) and gastrocnemius (lower panel) by fitting to both a Voigt lineshape and by FOM. IMCL/EMCL was approximately the same in lean muscle by both methods. However, in muscle with high EMCL, FOM returned significantly lower values.

Table 1: Comparison of IMCL concentration as results from fitting with a Voigt Lineshape and Fiber Orientation Modeling

Patients #	**IMCL Concentration** (mmol/kg wet weight)	
	FOM	**Voigt**
Gastroc1	1.6750419	2.0100503
Gastroc2	4.0201005	6.4608758
Gastroc3	1.7587940	2.2613065
Gastroc4	1.6750419	2.2140443
Gastroc5	3.0150754	8.5985483
Gastroc6	8.2914573	27.1356784
Gastroc7	3.2470043	5.0251256
Gastroc8	5.8368767	11.0552764
Gastroc9	4.0201005	10.0502513
Average:	**3.7266103**	**8.3123508**
Standard Deviation:	**2.1934504**	**7.8477767**
Soleus1	9.7989950	14.1959799
Soleus2	5.1164915	13.7048881
Soleus3	3.3243139	7.9371215
Soleus4	4.3293390	10.3788172
Soleus5	3.7108620	8.8906069
Soleus6	3.5298443	8.3343547
Soleus7	3.3442873	15.5778894
Soleus8	2.2696744	6.1737258
Average:	**4.4279759**	**10.6491729**
Standard Deviation:	**2.3208138**	**3.4250831**

CHAPTER FOUR
Conclusions and Recommendations

The current work was motivated by the large residuals evident when fitting ^{1}H NMR spectra of gastrocnemius or soleus at 7T using a Voigt lineshape. Other investigators have observed asymmetry in the EMCL methylene resonance. Steidle et al. suggested a method of separating IMCL from an overlapping EMCL signal by estimating magnetic field distribution with a reference spectrum obtained from bone marrow and assuming that the IMCL signal had the same linewidth as an aqueous metabolite, creatine [24]. Weis et al. obtained a reference EMCL spectrum by fitting a series of pure EMCL spectra [1]. This approach again required a reference spectrum from a different anatomical region.

We explored fiber orientation modeling (FOM) as an alternative approach to quantify the EMCL and IMCL signal that does not require a reference spectrum. Fitting both simulated spectra and real data with FOM produced smaller residuals. FOM was much less sensitive to dispersion of the orientation of extracellular lipids compared to fitting with symmetric lineshapes. In simulations with a dominant angle of 10° or less relative to the applied field and little dispersion, Voigt lineshape accurately determined IMCL/EMCL ratio. Even at a dispersion of 20° with a dominant angle parallel to Bo, Voigt lineshape analysis was accurate. In additional simulations (data not shown) the linewidth and lineshape (Gaussian vs. Lorentzian) of the EMCL and IMCL signals had little effect on the accuracy of IMCL estimates with a dominant angle less than 10° and little dispersion. Together, these results are consistent with the general consensus that spectra from the anterior tibialis (where the muscle fibers are predominantly parallel to Bo) may be analyzed confidently [14].

Standard models and experimental data [11, 26] demonstrate that as EMCL approaches an orientation of about 54° relative to Bo, EMCL protons coresonate with IMCL protons. Since muscle fibers and presumably fatty strands between those fibers are generally not parallel to Bo or to one another, asymmetry of the EMCL signal and overlap with the IMCL resonances should be expected. The challenge is to quantify IMCL in the presence of this overlap. In effect, FOM uses amplitude information from resonances well-resolved from the IMCL signal (near 0° relative to Bo) to estimate the dominant angle of extracellular fat and the width of the Gaussian function used to describe orientation of EMCL as it varies smoothly from 0 to 90°. With this information, it is possible to estimate the contribution of EMCL to the signal assigned to IMCL.

The calculated [IMCL] in human subjects using FOM was less than half the value calculated using a Voigt lineshape. The analysis of simulated spectra suggests that this approach is essential, at least for data acquired at 7T. The [IMCL] in soleus observed using FOM, about 4.43 mmol/kg wet weight, is somewhat less than the values at lower fields where [IMCL] was 10.7 mmol/kg wet weight (at 1.5 T, ref. 12), 10.3 mmol/kg wet weight (at 1.5 T, ref. 20), or 7.6 mmol/kg wet weight (at 4.0 T, ref. 19). Hwang et al., also working at 4.0 T, reported [IMCL] of 4.8 mmol/kg wet weight, very similar to our finding [21]. Gaussian lineshapes were used in the fitting. However, the linewidth of the IMCL signal was not determined by fitting but rather was fixed at the linewidth of the methyl resonance of creatine, a process that conceivably reduces the estimated area of the IMCL signal.

A high concentration of IMCL may predispose a person to type 2 diabetes, and it is known that the amplitude of the resonance assigned to IMCL methylene protons is increased in subjects with insulin resistance [22, 23, 30]. Somewhat paradoxically, the amplitude of this signal is also increased among highly-trained endurance athletes who are exquisitely sensitive to

insulin [30]. The relevance of the current results at 7T to studies at lower field is unknown, but these data stress that the three-dimensional structure of fat in the extracellular compartment strongly influence the apparent quantity of IMCL.

CHAPTER FIVE
Applications and Future Directions

Diabetes Mellitus (DM) is a major cause of morbidity and mortality in United States. In 2004, diabetes ranked as 6th leading cause with 64,747 deaths [31]. Insulin resistance, a typical characteristic of type II DM, has been linked to the abnormalities in glucose and lipid metabolism. As a major site for insulin-stimulated glucose uptake and utilization, skeletal muscle's reduced ability to respond to insulin signal is considered to be sign of metabolic syndrome and pre-diabetic state [32].In muscle tissue, lipids are stored as extramyocellular lipids (EMCL), interstitial adipocytes between muscle fibers, or as intramyocellular lipids (IMCL), fat droplets accumulate in the muscle cytoplasm [29]. In contrast to EMCL, which have slow turn-over rate and metabolically inert, IMCL is mobilized and used in much shorter period of time, usually within several hours [22]. As the result, researches focused in this area suggested that the accumulation of metabolically active IMCL might interfere with insulin signal for glucose metabolism and were associated with insulin resistance in human [14]. Recently, Lee et al. [33] suggested that saturated, but not polyunsaturated, fatty acids induce insulin resistance in animal models.

Insulin resistance was also linked to mitochondrial dysfunction. The mitochondria play an essential in energy homeostasis by oxidative metabolism, producing ATP as energy for the body. Imbalance between energy intake and expenditure leads to mitochondrial dysfunction [34]. Genetic factors and environmental factors including exercise, diet, aging, and oxidative stress may affect mitochondrial function [35, 36]. There is evidence in recent literature suggesting that

mitochondrial dysfunction is associated with type 2 diabetes and insulin resistance in skeletal muscle [37- 39] and also in other tissues like liver, heart and pancreas [40-42]. Mitochondrial dysfunction results in accumulation of fatty acid metabolites, DG, and long-chain fatty acyl-CoA (LCFA-CoA) [43]. Circulating free fatty acids (FFAs), elevated during stress, or excess energy intake also lead to accumulation of FFAs, diacylglycerol (DG), and triglycerides in nonadipose tissue, including skeletal muscle, liver, heart, and β-cells. The accumulation can activated PKCs resulting increased in phosphorylation of insulin receptor substrate, leading to inhibition of insulin signaling and insulin resistance [43-45].

The ultimate goal of our study is to understand the pathogenesis of insulin resistance due to impaired mitochondrial oxidative function resulting in accumulation of intramyocellular lipids using NMR techniques under high-strength magnetic field (7 Tesla). This project requires multiple-pronged approach (as illustrated in Figure 10):

- Accurately defined IMCL concentration by ^{1}H spectroscopy (as presented in this thesis)
- IMCL composition and TCA cycle kinetics by ^{13}C NMR with ^{1}H decoupling
- ATP synthesis by ^{31}P magnetization transfer and ^{1}H decoupling

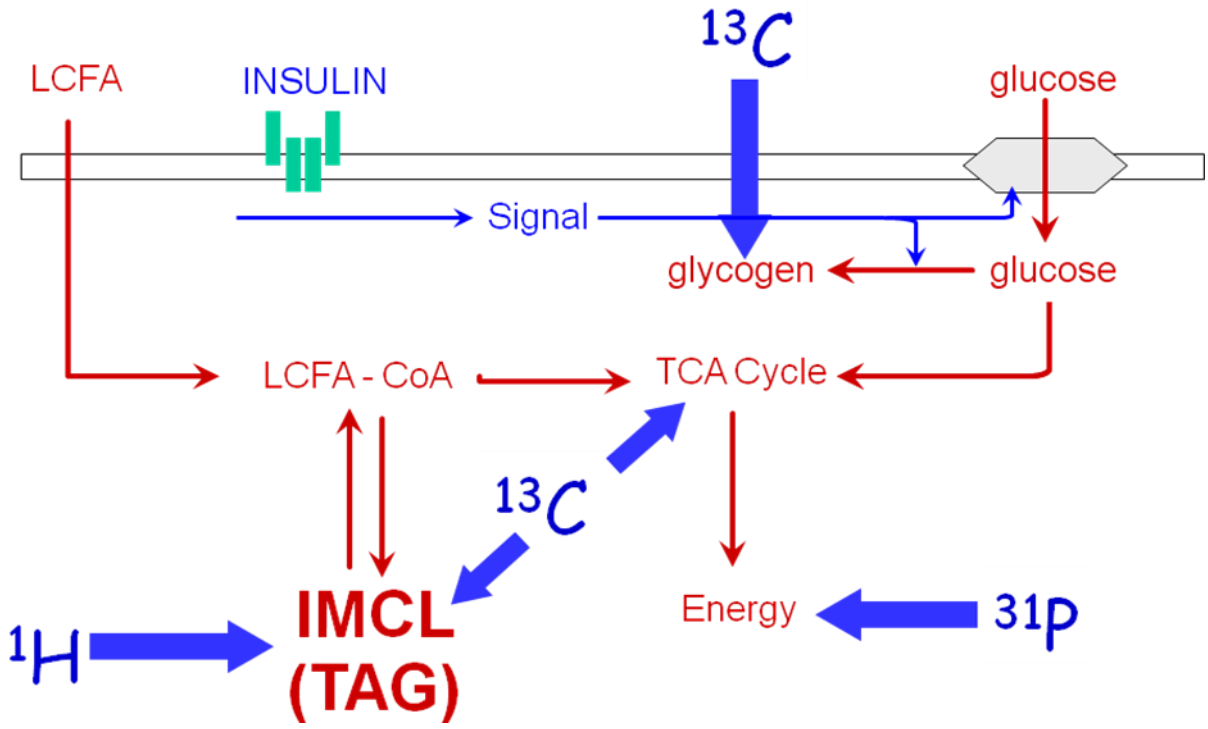

Figure 10: Technical Objectives of Skeletal Muscle Studies at 7T in Human Subjects

BIBLIOGRAPHY

1. **Weis J, Courivaud F, Hansen MS, Johansson L, Ribe LR, Ahlstrom H.** Lipid content in the musculature of the lower leg: evaluation with high-resolution spectroscopic imaging. Magn Reson Med. 2005; 54: 152-8.

2. **Schick F, Eismann B, Jung WI, Bongers H, Bunse M, Lutz O.** Comparison of localized proton NMR signals of skeletal muscle and fat tissue in vivo: two lipid compartments in muscle tissue. Magn Reson Med. 1993; 29: 158-67.

3. **Boesch C, Machann J, Vermathen P, Schick F**. Role of proton MR for the study of muscle lipid metabolism. NMR Biomed. 2006; 19: 968-88.

4. **Boesch C.** Musculoskeletal spectroscopy. J Magn Reson Imaging. 2007; 25: 321-38.

5. **Boesch C, Slotboom H, Hoppeler H, Kreis R.** In vivo determination of intra-myocellular lipids in human muscle by means of localized ^{1}H-MR-spectroscopy. Magn. Reson. Med. 1997; 37: 484-493.

6. **Klein MP, Phelps DE.** Evidence against orientation of water in rat phrenic nerve. Nature. 1969; 224: 70-1.

7. **Barbara TM.** Cylindrical demagnetization fields and microprobe design in high-resolution NMR. J Magn Reson Series A 1994; 109: 265-269.

8. **Chu SC, Xu Y, Balschi JA, Springer CS Jr.** Bulk magnetic susceptibility shifts in NMR studies of compartmentalized samples: use of paramagnetic reagents. Magn Reson Med. 1990; 13: 239-62.

9. **Ulrich R, Glaser RW, Ulrich AS.** Susceptibility corrections in solid state NMR experiments with oriented membrane samples. Part II: theory. J Magn Reson. 2003; 164: 115-27.

10. **Boesch C, Decombaz J, Slotboom J, Kreis R.** Observation of intramyocellular lipids by means of ^{1}H magnetic resonance spectroscopy. Proc Nutr Soc. 1999; 58: 841-50.

11. **Szczepaniak LS, Dobbins RL, Stein DT, McGarry JD.** Bulk magnetic susceptibility effects on the assessment of intra- and extramyocellular lipids in vivo. Magn Reson Med. 2002; 47: 607-10.

12. **Szczepaniak LS, Babcock EE, Schick F, Dobbins RL, Garg A, Burns DK, McGarry JD, Stein DT.** Measurement of intracellular triglyceride stores by H spectroscopy: validation in vivo. Am J Physiol. 1999; 276: E977-89.

13. **Kreis R, Boesch C.** Spatially localized, one- and two-dimensional NMR spectroscopy and in vivo application to human muscle. J Magn Reson B. 1996; 113: 103-18.

14. **Machann J, Haring H, Schick F, Stumvoll M**. Intramyocellular lipids and insulin resistance. Diabetes Obes Metab. 2004; 6: 239-48.

15. **Howald H, Boesch C, Kreis R, Matter S, Billeter R, Essen-Gustavsson B, Hoppeler H.** Content of intramyocellular lipids derived by electron microscopy, biochemical assays, and (1)H-MR spectroscopy. J Appl Physiol. 2002; 92: 2264-72.

16. **Larson-Meyer DE, Newcomer BR, Hunter GR.** Influence of endurance running and recovery diet on intramyocellular lipid content in women: a ^{1}H NMR study. Am J Physiol Endocrinol Metab. 2002; 282: E95-E106.

17. **Befroy DE, Petersen KF, Dufour S, Mason GF, de Graaf RA, Rothman DL, Shulman GI.** Impaired mitochondrial substrate oxidation in muscle of insulin-resistant offspring of type 2 diabetic patients. Diabetes. 2007; 56: 1376-81.

18. **Petersen KF, Dufour S, Befroy D, Garcia R, Shulman GI**. Impaired mitochondrial activity in the insulin-resistant offspring of patients with type 2 diabetes. N Engl J Med. 2004; 350: 664-71.

19. **Cui MH, Hwang JH, Tomuta V, Dong Z, Stein DT.** Cross contamination of intramyocellular lipid signals through loss of bulk magnetic susceptibility effect differences in human muscle using (1)H-MRSI at 4 T. J Appl Physiol. 2007; 103: 1290-8.

20. **Rico-Sanz J, Thomas EL, Jenkinson G, Mierisová S, Iles R, Bell JD.** Diversity in levels of intracellular total creatine and triglycerides in human skeletal muscles observed by (1)H-MRS. J Appl Physiol. 1999; 87: 2068-72.

21. **Hwang JH, Pan JW, Heydari S, Hetherington HP, Stein DT.** Regional differences in intramyocellular lipids in humans observed by in vivo ^{1}H-MR spectroscopic imaging. J Appl Physiol. 2001; 90: 1267-74.

22. **Krssak M, Falk Petersen K, Dresner A, DiPietro L, Vogel SM, Rothman DL, Roden M, Shulman GI**. Intramyocellular lipid concentrations are correlated with insulin sensitivity in humans: a ^{1}H NMR spectroscopy study. Diabetologia. 1999; 42: 113-6.

23. **Jacob S, Machann J, Rett K, Brechtel K, Volk A, Renn W, Maerker E, Matthaei S, Schick F, Claussen CD, Haring HU**. Association of increased intramyocellular lipid content with insulin resistance in lean nondiabetic offspring of type 2 diabetic subjects. Diabetes. 1999; 48: 1113-9.

24. **Steidle G, Machann J, Claussen CD, Schick F**. Separation of intra- and extramyocellular lipid signals in proton MR spectra by determination of their magnetic field distribution. J Magn Reson. 2002; 154: 228-35.

25. **Vermathen P, Boesch C, Kreis R.** Mapping fiber orientation in human muscle by proton MR spectroscopic imaging. Magn Reson Med. 2003; 49: 424-32.

26. **Kim SG and Bandettini PA,** Principles of Functional MRI, in Functional MRI: Basic Principles and Clinical Applications, SH Faro and FB Mohamed, Eds., Springer, 2006, pp 3 - 23.

27. **Soher BJ, Hurd RE, Sailasuta N, Barker PB.** Quantitation of automated single-voxel proton MRS using cerebral water as an internal reference. Magn Reson Med. 1996; 36: 335-9.

28. **Vermathen P, Kreis R, Boesch C**. Distribution of intramyocellular lipids in human calf muscles as determined by MR spectroscopic imaging. Magn Reson Med. 2004; 51: 253-62.

29. **Field CJ, Angel A, Clandinin MT**. Relationship of diet to the fatty acid composition of human adipose tissue structural and stored lipids. Am J Clin Nutr. 1985; 42: 1206-20.

30. **van Loon LJ, Goodpaster BH**. Increased intramuscular lipid storage in the insulin-resistant and endurance-trained state. Pflugers Arch. 2006; 451: 606-16.

31. **Minino AM, Heron MP, Smith BL.** Deaths: preliminary data for 2004. Natl Vital Stat Rep, 2006. 54(19): p. 1-49.

32. **Baron AD, Brechtel G, Wallace P and Edelman SV**. Rates and tissue sites of non-insulin- and insulin-mediated glucose uptake in humans. Am J Physiol, 1988. 255(6 Pt 1): p. E769-74.

33. **Lee JS, Pinnamaneni SK, Eo SJ, Cho IH, Pyo JH, Kim CK, Sinclair AJ, Febbraio MA, Watt MJ**. Saturated, but not n-6 polyunsaturated, fatty acids induce insulin resistance: role of intramuscular accumulation of lipid metabolites. J Appl Physiol 2006;100:1467-74

34. **Brehm A, Krssak M, Schmid AI, Nowotny P, Waldhausl W, Roden M.** Increased lipid availability impairs insulin-stimulated ATP synthesis in human skeletal muscle. Diabetes. 2006;55:136 –140.

35. **Ritz P, Berrut G.** Mitochondrial function, energy expenditure, aging and insulin resistance. Diabetes Metab. 2005;31(Spec No 2):5S67–5S73.

36. **Frisard M, Ravussin E.** Energy metabolism and oxidative stress: impact on the metabolic syndrome and the aging process. Endocrine. 2006;29:27–32

37. **Stump CS, Short KR, Bigelow ML, Schimke JM, Nair KS.** Effect of insulin on human skeletal muscle mitochondrial ATP production, protein synthesis, and mRNA transcripts. Proc Natl Acad Sci U S A. 2003;100:7996–8001.

38. **Petersen KF, Befroy D, Dufour S, Dziura J, Ariyan C, Rothman DL, DiPietro L, Cline GW, Shulman GI.** Mitochondrial dysfunction in the elderly: possible role in insulin resistance. Science. 2003;300: 1140–1142.

39. **Mogensen M, Sahlin K, Fernstrom M, Glintborg D, Vind BF, Beck-Nielsen H, Hojlund K.** Mitochondrial respiration is decreased in skeletal muscle of patients with type 2 diabetes. Diabetes. 2007;56:1592–1599.

40. **Ashrafian H, Frenneaux MP, Opie LH.** Metabolic mechanisms in heart failure. Circulation. 2007;116:434–448.

41. **Nisoli E, Clementi E, Carruba MO, Moncada S.** Defective mitochondrial biogenesis: a hallmark of the high cardiovascular risk in the metabolic syndrome? Circ Res. 2007;100:795– 806.

42. **Wiederkehr A, Wollheim CB.** Minireview: implication of mitochondria in insulin secretion and action. Endocrinology. 2006;147:2643–2649.

43. **Itani SI, Ruderman NB, Schmieder F, Boden G.** Lipid-induced insulin resistance in human muscle is associated with changes in diacylglycerol, protein kinase C, and IkappaB-alpha. Diabetes. 2002;51:2005–2011.

44. **Yu C, Chen Y, Cline GW, Zhang D, Zong H, Wang Y, Bergeron R, Kim JK, Cushman SW, Cooney GJ, Atcheson B, White MF, Kraegen EW, Shulman GI.** Mechanism by which fatty acids inhibit insulin activation of insulin receptor substrate-1 (IRS-1)-associated phosphatidylinositol 3-kinase activity in muscle. J Biol Chem. 2002;277:50230 –50236.

45. **Griffin ME, Marcucci MJ, Cline GW, Bell K, Barucci N, Lee D, Goodyear LJ, Kraegen EW, White MF, Shulman GI.** Free fatty acidinduced insulin resistance is associated with activation of protein kinase C theta and alterations in the insulin signaling cascade. Diabetes. 1999; 48:1270 –1274.

Vitae

Anthony N. Khuu was born in Saigon, Vietnam on July 27, 1984 to Khuu Tang The and Nguyen Thi Thanh Nhan. After completing his work at Bui Thi Xuan High School, Vietnam in 2002, Anthony and his parent migrated from Vietnam to the United States. He spent his first year in a new country working alongside his parent in factory while waiting table in the weekend at a local Chinese restaurant. Prior to transferring to The University of Texas at Arlington, he earned 60 hours of college credit in one year at Tarrant County Community College with a 4.0 GPA while working as a lab assistant in the school's Chemistry department. He was named to the Dean's List and All "A" Honor Roll in all semester at The University of Texas at Arlington. During these undergraduate years, he was also engaging in numerous extracurricular activities, focusing in teaching and community services. He was a teaching assistant in Biology I and II, Organic Chemistry and Microbiology in most semesters at the school; participating in National Society of Collegiate Scholars, Golden Key honor society, Phi Beta Kappa honor society. Along with teaching, he has a keen interest in botany and ecology, presenting a poster at a Science Fair in the Department of Biology on topic of "Urban Heat Islands and mitigating solutions from local plants". He has also served his community through volunteer activities at the John Peter Smith Hospital in Fort Worth as a pharmacy clerk while maintaining his weekend job at a local restaurant. After two year in The University of Texas at Arlington, Anthony graduated *summa cum laude* with a Bachelor of Science degree in Biology in 2006.

In August of 2006, Anthony entered medical school at the University of Texas Southwestern Medical School. Anthony's extracurricular interests during medical school balance his newfound passions for music, photography, language and community services. He taught himself playing piano with books and vast internet resources. He has keen interest in still-life photography, using his lens to capture plants and wildlife of North Texas. As time allows, he has volunteered at several events such as Holiday in the Park, providing children in underserved community of Dallas with a holiday festival and the annual United to Serves, a event that provide free health screening and health educational information to the

indigent community around the medical school. Additionally, he worked regularly on campus at Bryan Williams, M.D. Student Center as a front desk clerk and help preparing several campus events as an employee. During his senior year, Anthony again fulfills his passion for teaching by being a tutor for the clinical portion of MED-1901 summer course for rising first year and second year medical students. The Clinical Medicine portion of the course is brand new and he is fully in charge of constructing the curriculum and syllabus.

Anthony has also been very involved in research since the summer of his first year. He participated in the summer research program working with Craig R. Malloy, M.D. in the Advanced Imaging Research Center of the Department of Radiology. The project has ignited his passion for radiology research. His work then extended beyond the summer into second, third and fourth years where he worked countless hours on his personal computer at night for the project. Not only did he participated heavily in the formulation and completion of a new model (Fiber Orientation Modeling) for processing Magnetic Resonance Spectroscopy of intracellular lipid, he self-taught software programming to design a user-friendly program for further utilization of the algorithm in other projects. He is currently working several investigators on utilize the program for their projects: Dr. Manisha Shah with Congestive Heart Failure project; Dr. Sailaja Golla with the MELAS project and Dr. Katja Heinicke with project on mitochondrial myopathies. The research resulted in a first authorship on a publication in the *Magnetic Resonance in Medicine in* 2008 and co-authorship on two others currently in draft. Posters from this project had also been presented at Annual Medical Student Research Forum in 2007 and at the International Society for Magnetic Resonance in Medicine in 2008.

Anthony will complete his Doctorate of Medicine with Distinction in Research in June of 2010 and will pursue a career in Diagnostic Radiology.